Z. Angew. Math. Phys. (2023) 74:61

0044-2275/23/020001-11
published online February 16, 2023
https://doi.org/10.1007/s00033-023-01947-5

Zeitschrift für angewandte Mathematik und Physik ZAMP

Interface crack behaviors disturbed by Love waves in a 1D hexagonal quasicrystal coating–substrate structure

Yuanyuan Ma, Yueting Zhou, Juan Yang, Xuefen Zhao and Shenghu Ding

Abstract. The scattering of Love waves by an interface crack between a one-dimensional (1D) hexagonal quasicrystal (QC) coating and a half-space elastic substrate is investigated by using the superposition principle and integral transform technique. Introducing the dislocation density function, the wave scattering problem is transformed into the Cauchy singular integral equations, and the dynamic stress intensity factors (SIFs) of the left and right crack tips are solved. By degrading the quasicrystalline coating to the elastic dielectric layer, the correctness of the present numerical results is verified compared to the classical one. Then, the effects of the material combinations, incidence direction, crack sizes, and coupling coefficient on the dynamic SIFs are analyzed. The results show that the appropriate material combinations and incidence direction can hinder crack expansion. Moreover, the smaller the absolute value of the coupling coefficient and the crack sizes, the smaller the peak and volatility of the dynamic SIFs. The conclusions of this paper provide a theoretical basis for the dynamic failure analysis and nondestructive tests of QCs.

Mathematics Subject Classification. 42A38.

Keywords. 1D hexagonal QC coating, Love waves, Interface crack, Dynamic SIFs.

1. Introduction

As a new kind of materials, quasicrystals (QCs) have a wide range of excellent features owing to the special quasiperiodic structure [1,2]. Because of these features, they are widely used in the aerospace, and automotive industries, the solar thermal industry, energy engineering, and medical equipment [3,4]. However, it is found that QCs are brittle at normal temperatures, and the defects such as holes, cracks, and inclusions are easy to occur in the process of preparation [5], which may lead to structural damage and material failure. A large body of the literature has been developed for the fracture statics mechanics of QCs [6–9]. The dynamic deformation of QC structures is extremely complex due to the coupling of the phonon and phason fields, making relatively few studies on the fracture dynamics of QCs. With the increasing actual application needs, they are also attracting more and more attention. Two different kinetic models are used for dynamic deformation. One is the Bak's model [10], considering that the phason field is similar to the phonon field obeying Newton's second law. The other is the elasto-hydrodynamic model [11], which considers that the phason modes obey the diffusion law rather than the conservation law. Among them, the Bak's model is the most used by scholars owing to its simple mathematical description [12–15].

In recent years, elastic wave scattering has gradually become one of the most important research directions in elastic dynamics, and its application in nondestructive testing and evaluation of materials has a good background [16–18]. Because QCs are prone to defects such as cracks during manufacturing, the nondestructive testing technology for their structures has also attracted the attention of many scholars. Based on the elastodynamic equations of QCs, the analytical solution of the guided waves in the multilayered 1D hexagonal QC plates, functionally graded 1D hexagonal piezoelectric quasicrystal (PQC) plates, and a multilayered two-dimensional (2D) decagonal QC plate is investigated [19–21]. Wang and

Feng [22,23] studied the Lamb wave characteristics in functionally graded 1D hexagonal QC nanoplate and 2D PQC multilayered plates. Yang [24] studied the dynamic interaction between the SH wave and a crack in functionally graded 1D hexagonal PQCs by using the integral transform technique. Love wave is known as a surface acoustic wave with shear polarization that propagates as multiple total reflections in a layered waveguide of a given material deposited on a substrate with different elastic properties. It carries a lot of information about the physical parameters of the layer and substrate, which has a lot of characteristics such as wide amplitude, slow attenuation, and anti-interference [25,26]. In this case, Love wave is especially suitable for testing and evaluating the quality of the layer with a half-space structure. It has been successfully applied to the defect detection of crystal structures [27–29].

QCs are often applied as coatings or thin films on the surface of other materials [30,31]; therefore, the problem of interfacial cracking is more important in both engineering applications and theoretical analysis. However, the dynamic response of interfacial cracking in QCs has been poorly studied. In this paper, the response of an interfacial crack between a 1D hexagonal QC coating and an elastic substrate under the action of an incident Love wave is analyzed using the integral transform and the singular integral equation method. It will complement the existing research on elastic fracture theory and extend the application of classical integral transformations and potential functions to a wider and newer field, which is of great scientific significance and engineering application for the nondestructive testing of quasicrystal structures.

2. Problem description

The schematic diagram of a 1D hexagonal QC coating of infinite length and finite thickness h bonded to a semi-infinite elastic substrate is illustrated in Fig. 1. Using a Cartesian coordinate system(x, y, z), where the z-axis is the polarization direction of the 1D hexagonal QC coating, a central crack of length $2c$ is located on the x direction, and the Love wave incidents from the far side along the x-axis along the positive direction.

The anti-plane problem has the following assumptions:

$$\begin{aligned} &u_x = u_y = 0, \quad u_z = u_z(x, y, t), \\ &w_x = w_y = 0, \quad w_z = w_z(x, y, t), \\ &u_x^{\mathrm{e}} = u_y^{\mathrm{e}} = 0, \quad u_z^{\mathrm{e}} = u_z^{\mathrm{e}}(x, y, t). \end{aligned} \tag{1}$$

where u_i^{e} represents the displacement component of the elastic substrate, and u_i and w_i $(i = x,\ y,\ z)$ stand for the displacement components of the phonon field and phase field of the 1D hexagonal QC coating, respectively.

The constitutive relationships can be expressed as follows [19]:

$$\begin{cases} \sigma_{yz} = C_{44}\frac{\partial u_z}{\partial y} + R_3\frac{\partial w_z}{\partial y},\ \sigma_{xz} = C_{44}\frac{\partial u_z}{\partial x} + R_3\frac{\partial w_z}{\partial x}, \\ H_{zy} = R_3\frac{\partial u_z}{\partial y} + K_2\frac{\partial w_z}{\partial y},\ H_{zx} = R_3\frac{\partial u_z}{\partial x} + K_2\frac{\partial w_z}{\partial x}. \end{cases} \tag{2}$$

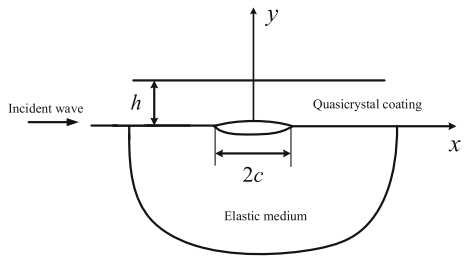

Fig. 1. An interface crack subjected to an incident Love wave

where σ_{iz} and $H_{zi}(i = x, y)$ represent the stress components of the phonon field and phason field; C_{44}, K_2, and R_3 are, respectively, elastic constants in the phonon and phason field, and phonon–phason field coupling constant.

In the context of the Bak's model, the kinetic equations without body forces are written as follows [19]:

$$\begin{cases} \frac{\partial \sigma_{zx}}{\partial x} + \frac{\partial \sigma_{zy}}{\partial y} = \rho \frac{\partial^2 u_z}{\partial t^2}, \\ \frac{\partial H_{zx}}{\partial x} + \frac{\partial H_{zy}}{\partial y} = \rho \frac{\partial^2 w_z}{\partial t^2}. \end{cases} \tag{3}$$

Substituting Eq. (2) into Eq. (3), the control equation for the 1D hexagonal QC coating can be written as

$$\begin{cases} C_{44}\nabla^2 u_z + R_3 \nabla^2 w_z = \rho \frac{\partial^2 u_z}{\partial t^2}, \\ R_3 \nabla^2 u_z + K_2 \nabla^2 w_z = \rho \frac{\partial^2 w_z}{\partial t^2}, \end{cases} \tag{4}$$

where $\nabla^2 = \frac{\partial^2}{\partial x^2} + \frac{\partial^2}{\partial y^2}$, ρ is the mass density of QCs, and t is the time.

In order to solve Eq. (4), introducing new displacement potential functions $\phi(x, y, t)$ and $\psi(x, y, t)$, these take the following forms:

$$u_z = a\phi - R_3\psi, w_z = R_3\phi + a\psi, \tag{5}$$

where $a = \frac{1}{2}\left[(C_{44} - K_2) + \sqrt{(C_{44} - K_2)^2 + 4R_3^2}\right]$, and Eq. (4) can be reduced to

$$\nabla^2\phi = \frac{1}{s_\phi^2}\frac{\partial^2\phi}{\partial t^2}, \nabla^2\psi = \frac{1}{s_\psi^2}\frac{\partial^2\psi}{\partial t^2}, \tag{6}$$

in which

$$s_\phi = \sqrt{(C_{44} + K_2) + \sqrt{(C_{44} - K_2)^2 + 4R_3^2}/2\rho},$$
$$s_\psi = \sqrt{(C_{44} + K_2) - \sqrt{(C_{44} - K_2)^2 + 4R_3^2}/2\rho},$$

are the velocities of shear waves traveling in the isotropic periodic plane of QCs.

Furthermore, the constitutive relationships and the kinetic equations of the elastic substrate can be expressed, respectively, as [28]:

$$\sigma_{z\alpha}^{\mathrm{e}} = c_{44}^{\mathrm{e}} u_{z,\alpha}^{\mathrm{e}}, (\alpha = x, y) \tag{7}$$

$$c_{44}^{\mathrm{e}}\nabla^2 u_z^{\mathrm{e}} = \rho^{e}\frac{\partial^2 u_z^{\mathrm{e}}}{\partial t^2}, (y < 0) \tag{8}$$

where c_{44}^{e} and ρ^{e} are the elastic stiffness and mass density of the elastic substrate.

3. Solutions to the problem

For the incident field problem, the solutions of Eqs. (6) and (8) have the following form:

$$\begin{aligned} \phi^{\mathrm{c}}(x, y, t) &= (A_1^c e^{\lambda_1 y} + A_2^c e^{-\lambda_1 y}) e^{i(kx-\omega t)}, \\ \psi^{\mathrm{c}}(x, y, t) &= (B_1^c e^{\lambda_2 y} + B_2^c e^{-\lambda_2 y}) e^{i(kx-\omega t)}, \\ u_z^{\mathrm{ec}}(x, y, t) &= C^{\mathrm{c}} e^{\lambda_3 y}\, e^{i(kx-\omega t)}, \end{aligned} \tag{9}$$

where the superscript "c" stands for quantities of the incident field, k is the wave number and ω is the circular frequency, A_1, A_2, B_1, B_2 and C are the constants to be solved, and the parameters λ_1, λ_2, and

λ_3 are given by

$$\lambda_1 = \sqrt{k^2 - \frac{\omega^2}{s_\phi^2}}, \lambda_2 = \sqrt{k^2 - \frac{\omega^2}{s_\psi^2}}, \lambda_3 = \sqrt{k^2 - \omega^2 \frac{\rho^e}{c_{44}^e}}. \tag{10}$$

The boundary conditions can be written as

$$\begin{array}{c} u_z^{\mathrm{c}}(x,0,t) = u_z^{\mathrm{ec}}(x,0,t), H_{yz}^{\mathrm{c}}(x,0,t) = 0, \\ \sigma_{yz}^{\mathrm{c}}(x,0,t) = \sigma_{yz}^{\mathrm{ec}}(x,0,t), \sigma_{yz}^{\mathrm{c}}(x,h,t) = 0, H_{yz}^{\mathrm{c}}(x,h,t) = 0. \end{array} \tag{11}$$

Inserting Eqs. (2), (7) and (9) into Eq. (11) leads to

$$\begin{array}{l} a(A_1^c + A_2^c) - R_3(B_1^c + B_2^c) = C^{\mathrm{c}}, \\ \left(C_{44}a + R_3^2\right)\lambda_1(A_1^c - A_2^c) + (R_3 a - C_{44}R_3)\lambda_2(B_1^c - B_2^c) = c_{44}^{\mathrm{e}}\lambda_3 C^{\mathrm{c}}, \\ (R_3 a + K_2 R_3)\lambda_1(A_1^c - A_2^c) + \left(K_2 a - R_3^2\right)\lambda_2(B_1^c - B_2^c) = 0, \\ \left(C_{44}a + R_3^2\right)\lambda_1(A_1^c e^{\lambda_1 h} - A_2^c e^{-\lambda_1 h}) + (R_3 a - C_{44}R_3)\lambda_2(B_1^c e^{\lambda_2 h} - B_2^c e^{-\lambda_2 h}) = 0, \\ (R_3 a + K_2 R_3)\lambda_1(A_1^c e^{\lambda_1 h} - A_2^c e^{-\lambda_1 h}) + \left(K_2 a - R_3^2\right)\lambda_2(B_1^c e^{\lambda_2 h} - B_2^c e^{-\lambda_2 h}) = 0. \end{array} \tag{12}$$

The existence of a nontrivial solution of Eq. (9) demands that the determinant value of the coefficient matrix H of Eq. (12) vanishes to be zero, producing the following frequency equation

$$\mathrm{Det}(\mathbf{H}) = 0. \tag{13}$$

The stress field in the crack position by the incident fields is obtained as

$$\tau(x,t) = \sigma_{yz}^{\mathrm{ec}}(x,0,t) = \tau_0 e^{i(kx-\omega t)}, \quad (-c < x < c) \tag{14}$$

where $\tau_0 = c_{44}^{\mathrm{e}}\lambda_3 C^{\mathrm{c}}$ and k is the wave number of the first mode. The time factor $e^{-i\omega t}$ is common to all the field variables in a steady-state regime, and so will be omitted in the sequel.

For the scattering fields problem, Fourier transformations of the coordinate variables x in Eqs. (6) and (8) give the solutions of the displacement and potential of the scattered field as

$$\begin{array}{l} \phi^{\mathrm{s}}(x,y) = \frac{1}{2\pi}\int_{-\infty}^{\infty}\left[A_1(s)e^{\lambda_1^s y} + A_2(s)e^{-\lambda_1^s y}\right]e^{-isx}\mathrm{d}s, \\ \psi^{\mathrm{s}}(x,y) = \frac{1}{2\pi}\int_{-\infty}^{\infty}\left[B_1(s)e^{\lambda_2^s y} + B_2(s)e^{-\lambda_2^s y}\right]e^{-isx}\mathrm{d}s, \\ u_z^{\mathrm{es}}(x,y) = \frac{1}{2\pi}\int_{-\infty}^{\infty} C_1(s)e^{\lambda_3^s y}e^{-isx}\mathrm{d}s, \end{array} \tag{15}$$

where the superscript "s" stands for quantities of the scattering fields, $A_1(s), A_2(s), B_1(s), B_2(s)$ and $C_1(s)$ are the functions to be solved, and the parameters λ_1, λ_2, and λ_3 obtained from Eq. (10) by replacing k with -s in Eq. (15) should satisfy the radiation condition and the finite condition at infinity, that is,

$$Re(\lambda_1^s, \lambda_2^s) < 0, Im(\lambda_1^s, \lambda_2^s) > 0, Re(\lambda_3^s) > 0, Im(\lambda_3^s) < 0.$$

The boundary conditions can be written as

$$\sigma_{yz}^{\mathrm{s}}(x,0) = \sigma_{yz}^{\mathrm{es}}(x,0) = -\tau(x), \quad H_{yz}^{\mathrm{s}}(x,0) = 0, (-c < x < c) \tag{16}$$

$$\sigma_{yz}^{\mathrm{s}}(x,0) = \sigma_{yz}^{\mathrm{es}}(x,0), H_{yz}^{\mathrm{s}}(x,0) = 0, u_z^{\mathrm{s}}(x,0) = u_z^{\mathrm{es}}(x,0), (|x| > c) \tag{17}$$

$$\sigma_{yz}^{\mathrm{s}}(x,h) = 0, \quad H_{zy}^{\mathrm{s}}(x,h) = 0, (-\infty < x < \infty) \tag{18}$$

Define the dislocation density function by

$$f(x) = \frac{\mathrm{d}[u_z^{\mathrm{s}}(x,0) - u_z^{\mathrm{es}}(x,0)]}{\mathrm{d}x}, \tag{19}$$

Using Eqs (2), (7), (15) and (19), the Cauchy singular integral equations of the first type are obtained from the boundary conditions (16)-(18),

$$\frac{M}{\pi}\int_{-c}^{c}\frac{f(t)}{t-x}\mathrm{d}t+\frac{1}{\pi}\int_{-c}^{c}f(t)\mathrm{d}t\int_{0}^{\infty}[kK_0(s)-M]\sin[s(t-x)]\mathrm{d}s=-\tau(x), \tag{20}$$

where

$$M=\lim_{s\to\infty}kK_0(s), kK_0(s)=-\lambda_3 c_{44}^{\mathrm{e}}\frac{D_{25}}{sD}. \tag{21}$$

where $D=\mathrm{Det}(\mathbf{H})$ can be obtained from Eq. (13) by replacing k with -s. D_{25} is a submatrix of D obtained by deleting all the components of the 2nd line and the 5th row.

The single value condition of Eq. (20) requires that

$$\int_{-c}^{c}f(t)\mathrm{d}t=0. \tag{22}$$

Introducing the dimensionless parameters $u=t/c$ and $r=x/c$, and making $f(t)=F(u)$, Eqs. (20) and (22) reduced to

$$\begin{array}{c}\frac{M}{\pi}\int_{-1}^{1}\frac{F(u)}{u-r}\mathrm{d}u+\frac{c}{\pi}\int_{-1}^{1}R(u,r)F(u)\mathrm{d}u=-\tau(r),\\ \int_{-1}^{1}F(u)\mathrm{d}u=0,\end{array} \tag{23}$$

where

$$R(u,r)=\int_{0}^{\infty}[kK_0(s)-M]\sin[sc(u-r)]\mathrm{d}s.$$

We define the following expression

$$F(u)=\frac{Q(u)}{\sqrt{1-u^2}},\quad Q(u)=\sum_{k=0}^{\infty}C_kT_k(u), \tag{24}$$

where $T_k(u)$ are the Chebyshev polynomials of the first kind. In the present paper, 40 terms in the summation of $Q(u)$ are taken to satisfy the demand for convergence sufficiently.

Using Eq. (24) and the Gauss–Chebyshev integral formula, the set of integral Eq. (23) is transformed into a system of linear algebraic equations as follows

$$\begin{array}{c}\sum_{l=1}^{N}[\frac{M}{u_l-r_m}+cR(u_l,r_m)]\frac{Q(u_l)}{N}=-\tau(r_m),\\ \sum_{l=1}^{N}\frac{Q(u_l)}{N}=0,\end{array} \tag{25}$$

where

$$\begin{array}{l}u_l=\cos(\frac{2l-1}{2N}\pi),(l=1,\ 2,...,N)\\ r_m=\cos(\frac{m}{N}\pi),(m=1,\ 2,...,N-1)\end{array} \tag{26}$$

Finally, the SIFs of the left and right crack tips are given by

$$\begin{array}{l}K_{\mathrm{III}}^{L}=\lim_{x\to-c^-}\sqrt{2(x+c)}\sigma_{yz}^{\mathrm{s}}(x,0)=\sqrt{c}\,MQ(-1),\\ K_{\mathrm{III}}^{R}=\lim_{x\to c^+}\sqrt{2(x-c)}\sigma_{yz}^{\mathrm{s}}(x,0)=-\sqrt{c}\,MQ(1).\end{array} \tag{27}$$

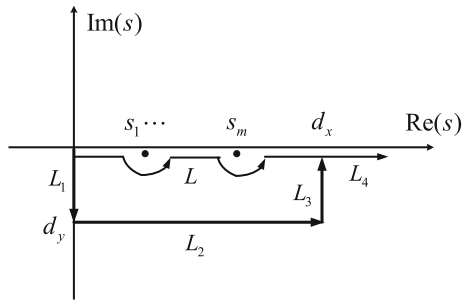

FIG. 2. Schematic diagram of the integral path

TABLE 1. *The material properties of the 1D hexagonal QCs and elastic substrate*

Material	C_{44} (N/m^2)	R_3 (N/m^2)	K_2 (N/m^2)	ρ(Kg/m^3)	C^e_{44}(N/m^2)
QC1	7.019×10^{10}	0.8864×10^9	2.4×10^{10}	4186	–
QC2	5.0×10^{10}	0.5×10^9	5.0×10^{10}	7500	–
Cu	–	–	–	8960	4.78×10^{10}
Al	–	–	–	2706	2.65×10^{10}

4. Results and discussion

It should be noticed that the integrands of Eq. (23) have some pole points in the integral path along the x-axis. So, the direct integral calculation along the x-axis is inappropriate and does not obtain the correct results. The offset path method is a simple and easy way to deal with the near-field problem of the crack tips [28]. As shown in Fig. 2, the poles, denoted as s_1, ..., s_m, are also the roots of Eq. (12). The parameters d_x and d_y, the deviation from the imaginary and the real axis, are defined as $d_x = 3\omega/2c_\mathrm{v}$ and $d_y = 0.05$. According to the path independence of the Cauchy integral formula, the correct integral results are obtained by following the integral contour consisting of L_1, L_2, L_3, and L_4.

The dimensionless parameters $\omega h/c_\mathrm{s}$ and $K_\mathrm{III}/K_\mathrm{III0}$ are introduced, where $K_\mathrm{III0} = \tau_0\sqrt{c}$ [24]. In addition, the dimensionless parameter c/h is introduced to characterize the crack size. For numerical calculation, the material properties of the 1D hexagonal QCs and elastic substrate are listed in Table 1 [19].

In this paper, the 1D hexagonal QC is degraded to the elastic material. The parameters $\omega h/c_\mathrm{s}$ curve of normalized SIFs of the elastic materials are compared to the Gu's solution [28], see Fig. 3. The result shows good agreement between the present numerical solution and Gu's, which demonstrates the validation of present numerical procedure.

The effect of different material combinations on the dynamic SIFs of the crack tips is given in Fig. 4, where $c/h = 2$. As can be seen that with the increase of $\omega h/c_\mathrm{s}$, the dynamic SIFs resonate at the low-frequency stage, reach a maximum value, and then decrease rapidly with further increase of $\omega h/c_\mathrm{s}$ with small oscillations occurring. For any crack tip, it is observed that the peak of dynamic SIFs in QC2/Al is smaller than those of QC1/Al, and the fluctuation is also smaller. That means the material is less prone to damage for the selection of QC2 coating when the substrate material is Al. On the contrary, the peaks of the primary and the secondary of the dynamic SIFs in the QC1/Cu are smaller than the results in the QC2/Cu; that is to say, when the substrate material is Cu, the material is not easily damaged by choosing QC1 coating. The comparison of different material combinations shows that the selection of suitable quasicrystalline coatings for different substrate materials can effectively reduce the dynamic SIFs at the crack tip, thus inhibiting the crack extension and improving the material properties.

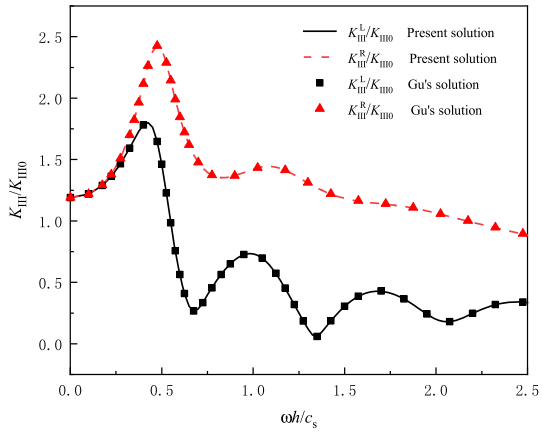

FIG. 3. Normalized SIFs versus $\omega h/c_s$ for elastic materials

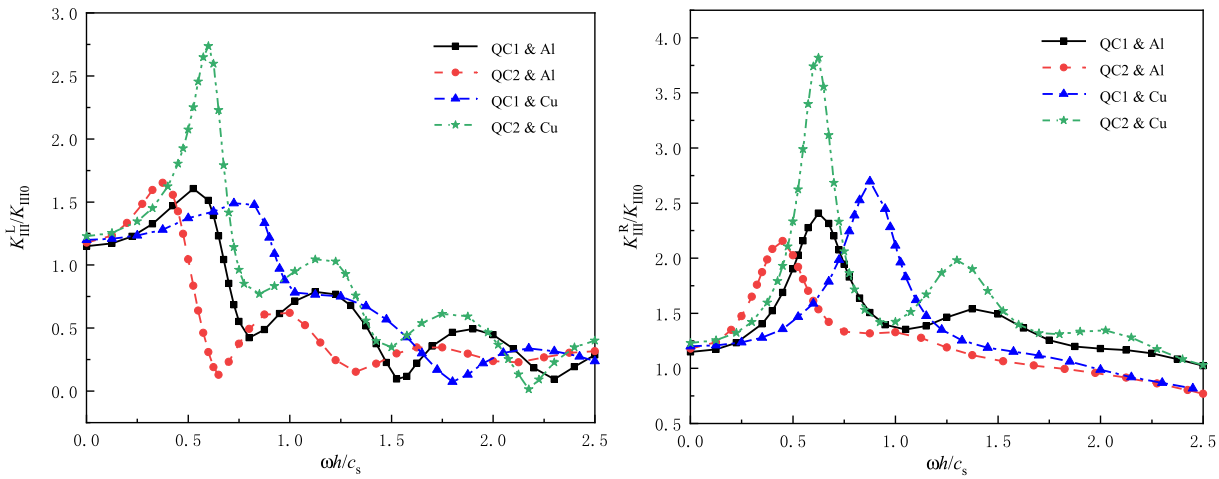

FIG. 4. The variation of K_{III}/K_{III0} with $\omega h/c_s$ for different material combinations

Figure 5 gives the variation of the dynamic SIFs with $\omega h/c_s$ for different crack tips. It can be seen that for any material combinations, the dynamic SIFs of the left and right crack tips are almost equal at the low-frequency stage before resonance, and as the frequency increases, the peak of the dynamic SIFs at the left crack tip is smaller than that at the right crack tip, but after reaching the peak, the fluctuation of the dynamic SIF of the left crack tip is stronger. This is because the incident wave propagates along the x-axis along the forward direction and encounters the left crack tip first, then scattering occurs at the crack, and the scattered and incident waves are superimposed on each other. The propagation direction of the incident wave has an important influence on the dynamic SIFs at the crack tips. In addition, the value of dynamic SIFs is smaller in the QC1/Cu when $\omega h/c_s < 0.6$, and the value and volatility of dynamic SIFs are smaller in the QC2/Al when $\omega h/c_s > 0.6$. Hence, for different frequencies, different material combinations can be selected to hinder crack expansion.

The effect of different crack sizes on the dynamic SIFs at the crack tips is shown in Fig. 6. It can be seen that the larger the value of c/h, the faster the dynamic SIFs reach their maximum values at the crack tips, and the larger the peak of the main oscillation peak. At the low-frequency stage, the smaller

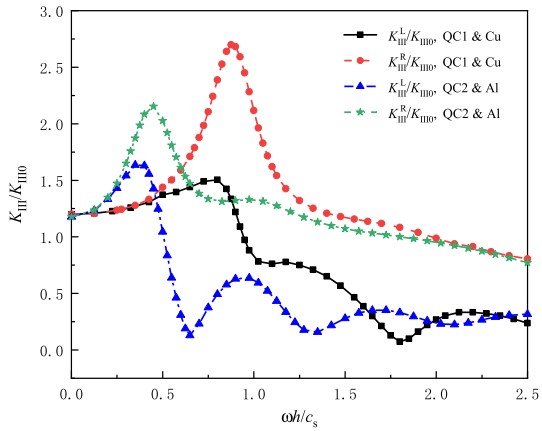

FIG. 5. The variation of K_{III}/K_{III0} with $\omega h/c_s$ for different crack tips

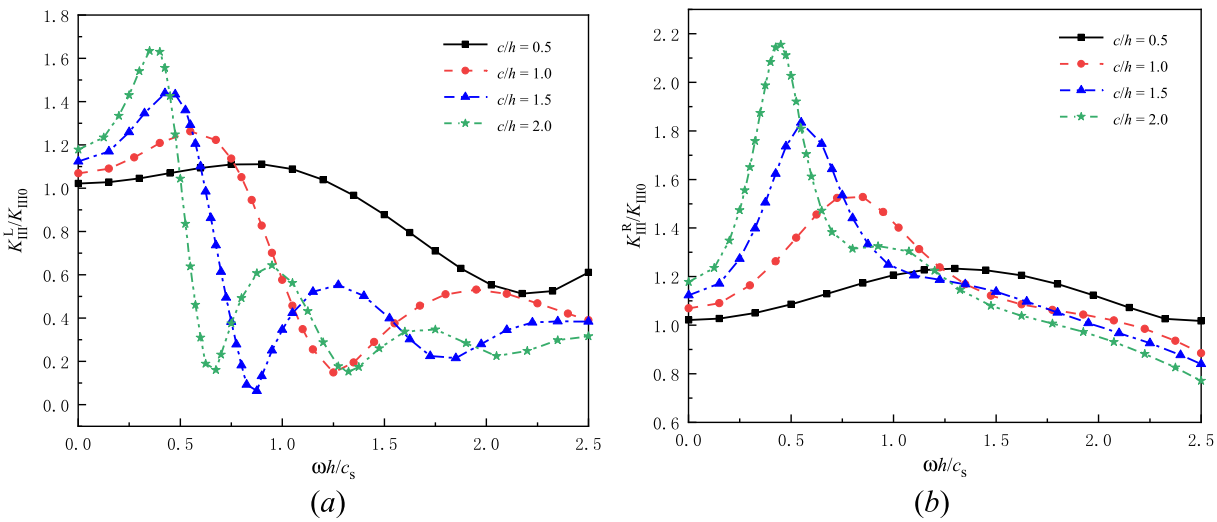

FIG. 6. The variation of K_{III}/K_{III0} with $\omega h/c_s$ for different crack sizes

the crack size, the smaller the dynamic SIFs at the crack tip. When $\omega h/c_s$ increases, the larger the crack size, the smaller the dynamic SIFs at the crack tip. It shows that the crack size has an important influence on the dynamic SIFs.

The variation of the dynamic SIFs with the coupling coefficient for the crack tips is given in Fig. 7, where $c/h = 2$. It can be found that the coupling coefficient has a small effect on the value of the dynamic SIFs at the crack tip. The reason for this can be seen in the expression $\sigma_{yz} = C_{44}\partial u_z/\partial y + R_3\partial w_z/\partial y$ of the stress, because the order of magnitude of the phonon field elastic constant C_{44} is 10^{10}, while order of magnitude of the phonon–phason field coupling constant R_3 is 10^9, which leads to a difference of one order of magnitude. From this, it is clear that the coupling constant has a small effect on its stress intensity factor. In addition, when the frequency is small, the dynamic SIFs of the crack tips are larger, but when the frequency is larger, the dynamic SIFs of the crack tips are smaller.

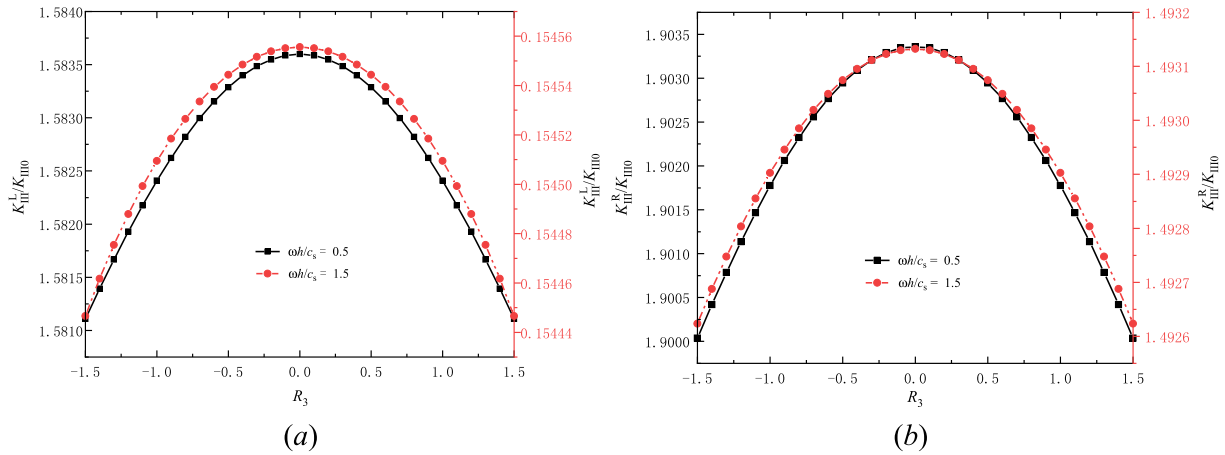

FIG. 7. The variation of K_{III}/K_{III0} with R_3 for different frequencies

5. Conclusion

The scattering problem of Love waves on an interfacial crack between a 1D hexagonal QC coating and an infinitely large homogeneous elastic substrate is investigated using the integral transform method. The dynamic SIFs near the crack tips determined from singular integral equations are obtained. The numerical results analyze the effects of material combination, incidence direction, crack sizes, and coupling coefficients on the dynamic SIFs. The results show that: (1) Different material combinations lead to variations of dynamic SIFs peaks and resonant frequencies at the crack tip, and the selection of appropriate material combinations can hinder crack expansion. (2) With the increase in crack sizes, the peak and volatility of the dynamic SIFs increase and the resonant frequency decreases. (3) The dynamic SIFs of the crack tip at one end of the incident direction are smaller than that at the other end, but the fluctuation is greater. (4) As the negative coupling coefficient increases, the dynamic SIFs at the crack tip gradually increase; conversely, as the positive coupling coefficient increases, the dynamic SIFs at the crack tip gradually decrease. These findings provide a theoretical basis for the nondestructive testing of quasicrystalline materials and the design of quasicrystalline materials.

Acknowledgements

This work was supported by National Natural Science Foundation of China (12262033, 12062021 and 12062022), Ningxia Hui Autonomous Region Science and Technology Innovation Leading Talent Training Project (KJT2020001), and the Natural Science Foundation of Ningxia (2022AAC03013; 2022AAC03068). Yueting Zhou would like to acknowledge the supports by the National Natural Foundation of China (11972257 and 12272269).

Author contributions YM, YZ, and XZ wrote the main manuscript text, and JY and SD prepared Figs. 1, 2, 3, 4, 5, 6, 7. All authors reviewed the manuscript.

Declaration

Conflict of interest On behalf all authors, the corresponding author states that there is no conflict of interest.

Publisher's Note Springer Nature remains neutral with regard to jurisdictional claims in published maps and institutional affiliations.

References

[1] Vekilov, Y.K., Isaev, E.I.: Quasicrystals: structure and properties. Crystall. Rep. **52**(6), 932–937 (2007)
[2] Lee, K., Chen, E., Naugle, D., et al.: Corrosive behavior of multi-phased quasicrystal alloys. J. Alloys Comp. **851**, 156862 (2020)
[3] Sanchez, A., de Blas, F.J.G., Algaba, J.M., et al.: Application of quasicrystalline materials as thermal barriers in aeronautics and future perspectives of use for these materials. Mater. Res. Soc. Symp. Proc. **553**, 447–458 (1999)
[4] Wang, Z.B., Ricoeur, A.: Numerical crack path prediction under mixed-mode loading in 1D quasicrystals. Theor. Appl. Fract. Mech. **90**, 122–132 (2017)
[5] Mompiou, F., Caillard, D.: Dislocations and mechanical properties of icosahedral quasicrystals. Comptes Rendus Physique **15**(1), 82–89 (2014)
[6] Yang, J., Li, X.: The anti-plane shear problem of two symmetric cracks originating from an elliptical hole in 1D hexagonal piezoelectric QCs. Adv. Mater. Res. **936**, 127–135 (2014)
[7] Fan, C.Y., Li, Y., Xu, G.T., et al.: Fundamental solutions and analysis of three-dimensional cracks in one-dimensional hexagonal piezoelectric quasicrystals. Mech. Res. Commun. **74**, 39–44 (2016)
[8] Hu, K.Q., Jin, H., Yang, Z.J., et al.: Interface crack between dissimilar one-dimensional hexagonal quasicrystals with piezoelectric effect. Acta Mech. **230**, 2455–2474 (2019)
[9] Zhai, T., Ma, Y.Y., Ding, S.H., et al.: Circular inclusion problem of two-dimensional decagonal quasicrystals with interfacial rigid lines under concentrated force. Zeitschrift fur Angewandte Mathematik und Mechanik **101**(12), e202100081 (2021)
[10] Bak, P.: Symmetry, stability, and elastic properties of icosahedral incommensurate crystals. Phys. Rev. B Condens. Matter **32**(9), 5764–5772 (1985)
[11] Lubensky, T.C., Ramaswamy, S., Toner, J.: Hydrodynamics of icosahedral quasicrystals. Phys. Rev. B Condens. Matter **32**(11), 7444–7452 (1985)
[12] Li, C.L., Liu, Y.Y.: Low-temperature lattice excitation of icosahedral Al-Mn-Pd quasicrystals. Phys. Rev. B **63**(6), 064203 (2001)
[13] Akmaz, H.K., Akinci, U.: On dynamic plane elasticity problems of 2D quasicrystals. Phys. Lett. A **373**(22), 1901–1905 (2009)
[14] Tupholme, G.E.: Row of shear cracks moving in one-dimensional hexagonal quasicrystalline materials. Eng. Fract. Mech. **134**, 451–458 (2015)
[15] Gao, Y.Y., Liu, G.T.: Analytic solutions of a fast propagating crack from triangular hole in 1D hexagonal piezoelectric quasicrystals. Math. Practice Theory **49**(11), 206–213 (2019). (**(in Chinese)**)
[16] Langenberg, K.J., Marklein, R.: Transient elastic waves applied to nondestructive testing of transversely isotropic lossless materials: a coordinate-free approach. Wave Motion **41**(3), 247–261 (2005)
[17] Yang, J., Li, X.: The scattering of the SH wave on a limited permeable crack in a functionally graded piezoelectric substrate bonded to a homogeneous piezoelectric strip. Acta Mech. **226**(10), 3205–3219 (2015)
[18] Potapov, A.I., Kondrat'ev, A.V., Smorodinskii, Y.G.: Nondestructive testing of structurally inhomogeneous composite materials by the method of elastic-wave velocity hodograph. Russian J. Nondestruct. Test. **55**(6), 434–442 (2019)
[19] Zhang, B., Yu, J.G., Zhang, X.M., et al.: Guided waves in the multilayered one-dimensional hexagonal quasi-crystal plates. Acta Mech. Solida Sin. **34**(1), 91–103 (2020)

[20] Zhang, B., Yu, J.G., Zhou, H.M., et al.: Guided waves in a functionally graded 1-D hexagonal quasi-crystal plate with piezoelectric effect. J. Intell. Mater. Syst. Struct. **33**(13), 1678–1696 (2022)
[21] Feng, X., Zhang, L.L., Hu, Z.M., et al.: Guided wave propagation in multilayered two-dimensional quasicrystal plates with imperfect interfaces. Acta Mech. Solida Sin. **35**(4), 694–704 (2022)
[22] Wang, X.X., Yu, J.G., Zhang, B., et al.: Lamb waves propagating in functionally graded 1-D quasi-crystal couple stress nanoplates. Acta Mech. **233**(8), 3021–3033 (2022)
[23] Feng, X., Zhang, J.M., Zhang, L.L, et al.: Lamb wave propagate in two-dimensional piezoelectric quasicrystal multilayered plates with nonlocal effect (2021). https://doi.org/10.1109/SPAWDA51471.2021.9445452
[24] Yang, J., Wang, X., Ding, S.H., et al.: Scattering of SH wave by a crack in a functionally graded one-dimensional hexagonal piezoelectric quasicrystals. ZAMM - Zeitschrift fur Angewandte Mathematik und Mechanik (2022). https://doi.org/10.1002/zamm.202200071
[25] Toshinawa, T., Ohmachi, T.: Love-wave propagation in a three-dimensional sedimentary basin. Bull. Seismol. Soc. Am. **82**(4), 1661–1677 (1992)
[26] Du, J., Harding, G.L., Collings, A.F., et al.: An experimental study of Love wave acoustic sensors operating in liquids. Sens. Actuators A Phys. **60**, 54–61 (1997)
[27] Liu, H., Wang, Z.K., Wang, T.J.: Effect of initial stress on the propagation behavior of Love waves in a layered piezoelectric structure. Int. J. Solids Struct. **38**(1), 37–51 (2001)
[28] Gu, B., Yu, S.W., Feng, X.Q., et al.: Scattering of love waves by an interface crack between a piezoelectric layer and an elastic substrate. Acta Mech. Solida Sin. **15**(2), 111–118 (2002)
[29] Li, X.Y., Wang, Z.K., Huang, S.H.: Love waves in functionally graded piezoelectric materials. Int. J. Solids Struct. **41**(26), 7309–7328 (2004)
[30] Guo, X.P., Chen, J.F., Yu, H.L., et al.: A study on the microstructure and tribological behavior of cold-sprayed metal matrix composites reinforced by particulate quasicrystal. Surface Coat. Technol. **268**, 94–98 (2015)
[31] Tian, Y., Huang, H., Yuan, G.Y., et al.: Microstructure evolution and mechanical properties of quasicrystal-reinforced Mg-Zn-Gd alloy processed by cyclic extrusion and compression. J. Alloys Comp. **626**, 42–48 (2015)

Yuanyuan Ma, Juan Yang, Xuefen Zhao and Shenghu Ding
School of Mathematics and Statistics
Ningxia University
Yinchuan 750021
China
e-mail: dshnx2019@nxu.edu.cn

Xuefen Zhao
Xinhua College
Ningxia University
Yinchuan 750021
China
e-mail: snownfen@163.com

Juan Yang
Institute of Ethnic Preparatory Education
Ningxia University
Yinchuan 750002
China

Yueting Zhou
School of Aerospace Engineering and Applied Mechanics
Tongji University
Shanghai 200092
China

(Received: December 26, 2022; revised: December 28, 2022; accepted: January 17, 2023)